This is a preprint of the following article, which is available from mdolab.engin.umich.edu
Eytan J. Adler and Joaquim R. R. A. Martins. Efficient Aerostructural Wing Optimization Considering Mission Analysis. *Journal of Aircraft*, 2022.
The original article may differ from this preprint and is available at
https://doi.org/10.2514/1.C037096.

Efficient Aerostructural Wing Optimization Considering Mission Analysis

Eytan J. Adler[1] and Joaquim R. R. A. Martins[2]
Department of Aerospace Engineering, University of Michigan, Ann Arbor, MI, 48109

Abstract

Aerostructural optimization traditionally uses a single or small number of cruise conditions to estimate the mission fuel burn objective function. In reality, a mission includes other flight segments contributing to fuel burn, such as climbing and descent. We aim to quantify how much performance is sacrificed by optimizing the design for a fuel burn approximation that ignores these other flight segments and flight conditions. To do this, we compare traditional approaches to mission-based optimization, which uses an accurate fuel burn objective computed by numerically integrating fuel flow across the mission profile. We find that mission-based optimization offers only marginal benefits over traditional single-point and multipoint approaches for aerostructural optimization of a narrowbody aircraft—only 1–2% in the most extreme cases. Thus, the traditional aerostructural optimization is acceptable, especially in cases where most fuel is burned during cruise. For the cases where climb fuel burn is significant, we introduce a simple change to traditional fuel burn approximation methods that allows the optimizer to find nearly all the fuel burn reduction of mission-based optimization but at the computational cost of multipoint optimization.

Nomenclature

L	=	lift
W	=	weight
D	=	drag
T	=	thrust
γ	=	flight path angle (positive for climb)
R	=	mission or mission segment range
V	=	flight speed
TSFC	=	thrust-specific fuel consumption
W_i	=	initial weight in a mission or mission segment
W_f	=	final weight in a mission or mission segment

[1]Ph.D. Candidate, AIAA Student Member
[2]Pauline M. Sherman Collegiate Professor, AIAA Fellow

1 Introduction

Quantifying the interaction between the aerodynamic performance and the structural behavior of an aircraft wing is integral to aircraft design. It facilitates the design of wings that strike the best balance of low weight and high aerodynamic performance—two closely-coupled and opposing objectives. Optimization of this aerostructural problem has been thoroughly researched. Haftka [1] was one of the first to investigate the coupled problem using low-fidelity, physics-based tools. Kenway et al. [2] accomplished it using Reynolds-averaged Navier–Stokes (RANS) computational fluid dynamics (CFD) and a detailed finite element analysis (FEA) model.

Early aerostructural optimizations minimized some combination of drag and structural weight [1, 3]. Replacing this objective with mission fuel burn combines drag and structural weight to minimize a more practical quantity. Most fuel-minimizing aerostructural optimizations fall into one of two categories. The first type, used in Kenway et al. [2], computes fuel burn based on the wing's performance at a single flight condition in cruise. This is referred to as single-point optimization. However, this approach often results in poor performance at other flight conditions. Multipoint aerostructural optimization, which followed single-point, addresses this by considering multiple cruise flight conditions in the objective function [4]. Both single-point and multipoint aerostructural formulations assume that most of the fuel is burned during cruise, that is, they assume that climb and descent fuel burn are negligible. The dominant cruise fuel burn assumption is necessary because they estimate total fuel burn with the Bréguet range equation, which assumes that the product of lift-to-drag ratio, airspeed, and thrust specific fuel consumption is constant throughout the mission. Thus, they perform all analyses at cruise flight conditions to compute the lift-to-drag ratio for the Bréguet range equation.

However, this cruise-only fuel burn calculation has been shown to differ from the actual mission fuel burn by 30% or more for short missions where climb fuel burn makes up a significant portion of the total mission fuel burn [5]. One way to account for this discrepancy in the climb and descent fuel burn is to use a correction factor based on the takeoff weight [6, 7]. Similarly, set fuel fractions could be used for non-cruise mission segments [8]. While these approaches are useful for conceptual design, they have a critical flaw for aerostructural optimization purposes. By excluding aerostructural analyses in climb, the optimizer does not know how subtle changes to the design will change the climb fuel burn. In other words, no analysis is performed in the climb when these corrections are used. This means that the optimizer could make a design change that marginally decreases cruise fuel burn while unaware that it massively increases climb fuel burn.

Previous work recognized that single-point and multipoint optimization problem formulations might not suit shorter missions. Liem et al. [9] identified the problem for regional jets and used numerical mission analysis coupled with a surrogate of the aerostructural model to compute the fuel burn objective function. Bons [10] highlighted the importance of considering climb and descent for high-fidelity regional jet aerostructural optimization. Bons modeled the mission fuel burn using low-fidelity approximations in climb and descent and high-fidelity analyses with the Bréguet range equation. Including climb and descent in the optimization offered important benefits, including a substantial drag decrease in climb and descent that is not achieved with a cruise-only Bréguet range objective. Chau and Zingg [11] performed high-fidelity aerostructural optimization of a regional jet and took a similar approach to Bons, using low-fidelity approximations to model mission segments outside of cruise. Clarke et al. [12] also observed that mission analysis gives a more complete understanding of aircraft performance than single-point formulations and accordingly used mission analysis to compute the objective function for coupled wing and propeller optimization.

This previous work raises a question: what is the penalty on the actual mission fuel burn caused by minimizing a single-point or multipoint fuel burn approximation based only on cruise

flight conditions? In other words, how much would actual fuel burn decrease by using a numerically-integrated fuel burn objective function that considers the full mission profile versus a single-point or multipoint approximation? The answer is crucial for high-fidelity aerostructural optimizations because it reveals how close their designs, which are optimized with the single-point and multipoint fuel burn approximations, are to the true optimum. In theory, the approximate fuel burn should approach the true mission fuel burn as the mission range increases and cruise fuel burn becomes more dominant. However, particularly for short missions flown by narrowbody and regional aircraft, when does the dominant fuel burn assumption break down? This has yet to be quantified in the literature.

To evaluate the effectiveness of traditional fuel burn objectives, we compare them against an actual mission fuel burn objective function. The actual mission fuel burn is computed by numerically integrating fuel flow across the mission profile, satisfying force balance at each integration point, and using a physics-based engine model. We refer to this method, which runs mission analysis in the loop, as mission-based optimization. It takes advantage of recent developments in fast aerostructural analysis with OpenAeroStruct[1] [13] and detailed, modular mission analysis with OpenConcept[2] [14]. All codes used in this work are open-source.

Mission-based optimization is not new to the field of aircraft design. However, using it for high-fidelity aerodynamic shape and aerostructural optimizations is a relatively recent development. Mission-based optimization has been widely used for conceptual aircraft design. NASA's Flight Optimization System (FLOPS) was developed in the early 1980s for this purpose [15]. Since then, various conceptual aircraft design optimization tools incorporating mission simulation have been developed. NASA developed LEAPS [16] to better model unconventional aircraft using physics-based models. The Aerospace Design Lab at Stanford created SUAVE [17] to be a modular way to design future aircraft. The MDO Lab at the University of Michigan developed OpenConcept [14], which takes advantage of analytic gradient methods to optimize designs efficiently. The Aerospace Systems Design Laboratory at Georgia Tech created GT-HEAT [18] to focus on propulsion system design. These mission-based tools have been used to optimize the design of a small UAV [19], the sizing of an electrified aircraft's thermal management system [20, 21], and the performance of a distributed propulsion system [22].

Incorporating CFD into mission-based optimizations is challenging because mission analysis requires tens to hundreds of aerodynamic evaluations throughout the mission. Solving the CFD at each point in the mission for every analysis would be prohibitively expensive. The most common approach to enable mission-based aerodynamic shape or aerostructural optimization with CFD is to use a surrogate of the CFD model in the mission analysis [9, 12, 23–26]. Thus, we use a similar approach.

By comparing traditional single and multipoint approaches to mission-based optimization, we show that optimized results from traditional approaches obtain actual mission fuel burns within 1% of the design from mission-based optimization. As expected, the advantage of mission-based optimization over traditional methods grows as the cruise distance decreases.

When climb fuel burn makes up a significant portion of the total fuel burn, we propose using a new objective function for high-fidelity aerostructural optimization that achieves most of the fuel burn benefit of mission-based optimization. Unlike traditional objective functions, it includes an analysis in climb to give the optimizer information about how design changes will affect climb performance. It achieves most of the fuel burn benefit of mission-based optimization at a fraction of the computational cost. The approach employs a modified Bréguet range equation, derived in

[1] https://github.com/mdolab/openaerostruct
[2] https://github.com/mdolab/openconcept

Section 5, that accounts for nonzero flight path angles. Two sequential evaluations of the modified equation are used to model the climb and cruise fuel burns. No analysis in descent is used because it has little impact on the optimized design due to the comparatively small amount of fuel burned in descent. This method achieves most of the benefits of mission-based optimization but with a lower computational cost than the multipoint optimization.

This paper is structured as follows. Section 2 discusses the models and methods with subsections describing OpenConcept, OpenAeroStruct, and the coupling of the two. Section 3 describes the optimization problems. Section 4 discusses the optimization results and compares them to previous methods. Section 5 describes our newly-proposed objective function for high-fidelity aerostructural optimization that better incorporates the effect of the climb with minimal additional computational cost.

2 Models and methods

The aerostructural mission analysis used in this work couples two existing codes: OpenConcept for the mission analysis and OpenAeroStruct for the aerostructural model. Both codes are open-source and built on the OpenMDAO framework [27], which enables the analysis and optimization of complex systems by harnessing analytic derivatives and the MAUD framework [28]. OpenAeroStruct's aerostructural model is incorporated into OpenConcept with a surrogate model, which offers a speedup compared to OpenConcept calling OpenAeroStruct directly.

2.1 Mission analysis (OpenConcept)

OpenConcept is a general-purpose conceptual aircraft design toolkit [14]. At its core, it uses numerical integrators to integrate aircraft states, such as fuel burn, over a customizable mission profile. At each numerical integration point, it selects the correct lift coefficient and engine throttle to balance forces. The model is solved all at once using a Newton solver that takes advantage of the built-in analytic derivatives to converge rapidly. The toolkit can handle complexity ranging from models with a simple parabolic drag polar and propulsion model to models using vortex lattice-based aerodynamics, parallel hybrid engine maps, and unsteady modeling of a battery and electric motor thermal management system [20].

The OpenConcept model in this work uses a CFM56 engine deck, which is a kriging surrogate of a pyCycle [29] model. OpenConcept uses OpenAeroStruct's vortex-lattice method (VLM) aerodynamic analysis and six-degree-of-freedom beam structural model for the aerostructural analysis. An eXtended Design Structure Matrix (XDSM) [30] of the OpenConcept mission analysis is shown in Figure 1. OpenConcept uses the drag from the OpenAeroStruct surrogate model, the thrust from the CFM56 engine deck, and the weight to solve for the lift and throttle needed to achieve zero acceleration at each numerical integration point in the mission. The aircraft design parameters, such as maximum takeoff weight and wing area, are based on the 737-800's design. Because OpenAeroStruct models only the wing, an estimate for the drag of the rest of the aircraft is required. This is done by matching the fuel burn to an equivalent OpenConcept model with an empirical parabolic drag polar of the 737-800 [31] instead of OpenAeroStruct's. This results in a zero lift drag coefficient of 0.0145 that is added to the drag from OpenAeroStruct. The wing weight returned by OpenAeroStruct is added to the OpenConcept model after subtracting the initial wing weight as estimated by Raymer [32].

The mission profile used for the results discussed in this paper is shown in Figure 2. The climb and descent segments have a set profile, and the cruise segment is at 35,000 ft and Mach 0.78 for its duration. The climb and descent profiles are roughly based on real-world data from similarly-sized

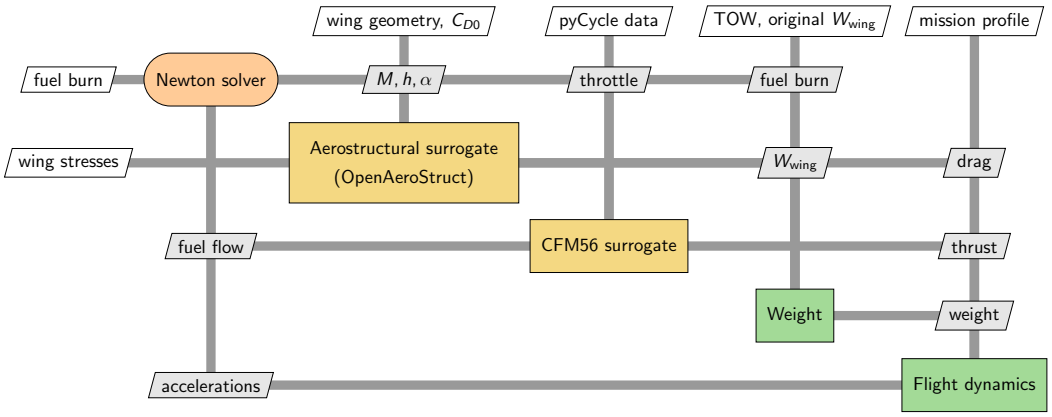

Figure 1: OpenConcept's mission analysis uses a Newton solver to converge the mission such that the acceleration at each numerical integration point is zero.

aircraft, though they are still contrived. The cruise segment is unrealistic for the 300 nmi mission since a lower cruise altitude would likely be chosen and is also unrealistic for longer missions because a step climb would be used as fuel is burned. The idea behind the chosen mission profile is not to perfectly represent a real-world mission but to provide a means for fairly comparing the different optimization methods in a way that is scalable to an arbitrary distance. Regardless of the mission length, the aircraft takes off at its maximum takeoff weight.

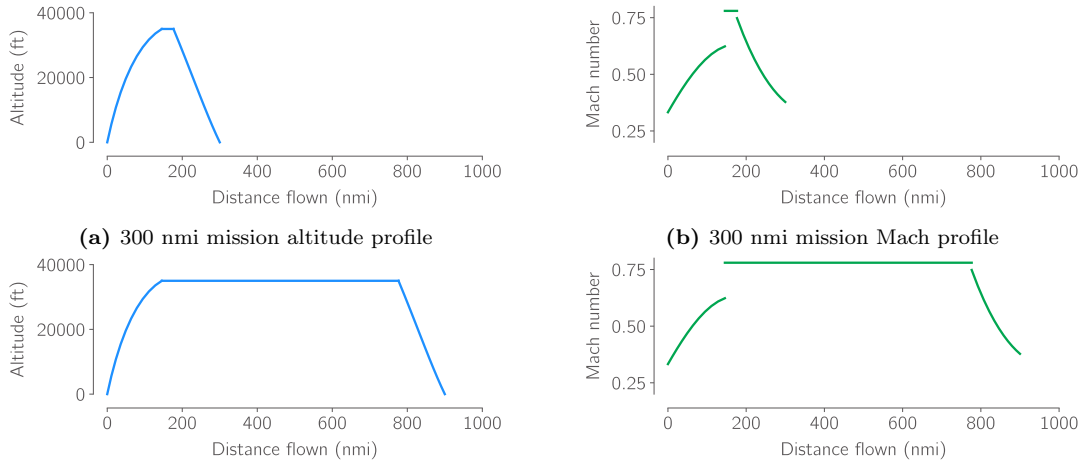

(a) 300 nmi mission altitude profile

(b) 300 nmi mission Mach profile

(c) 900 nmi mission altitude profile

(d) 900 nmi mission Mach profile

Figure 2: The mission profile consists of climb, cruise, and descent segments with the cruise at 35,000 ft and at Mach 0.78. The cruise segment is stretched until the mission reaches the desired length.

2.2 Aerostructural analysis (OpenAeroStruct)

OpenAeroStruct [13], the aerostructural analysis component, couples a vortex lattice aerodynamic model with a one-dimensional FEA model using six degree-of-freedom elements with axial, bending, and torsional stiffness. In this work, we use OpenAeroStruct's wingbox model [33], which computes the cross-sectional properties of airfoil-based wingbox cross-sections instead of the default tubular cross-section. OpenAeroStruct uses a semi-empirical model based on flat-plate

estimates and a form factor adjustment to account for skin friction and pressure drag. Finally, OpenAeroStruct includes a wave drag estimate based on the Korn equation. While the state-of-the-art in aerostructural optimization uses high-fidelity RANS CFD and a detailed FEA wingbox model, that approach requires thousands of core-hours for a single aerostructural optimization. Despite the lower fidelity, OpenAeroStruct has been shown to match closely with the higher fidelity cases [33]. The validation data from Chauhan and Martins [33] is shown in Table 1. Since it can perform aerostructural analysis in seconds, OpenAeroStruct enables rapid mission analysis of the wing and ultimately coupled aerostructural and mission profile optimization on a desktop computer.

	OpenAeroStruct [33]	High-fidelity [34]	Difference
Wing structural mass (kg)	21,467.66	23,840	−10.0%
Fuel burn (kg)	96,239.07	94,037	+2.3%

Table 1: Structural weight and fuel burn of a transport aircraft's wing optimized in OpenAeroStruct matches a high-fidelity aerostructural optimization result to within 10% [33].

The wing used in this work, shown in Figure 3, has a simple planform defined by area, aspect ratio, taper, and sweep. The planform area of 124.6 m^2 is the only parameter that is not modified by the optimizer. The wing also has an adjustable twist and thickness-to-chord ratio along the span. The wingbox model's structural sizing consists of skin and spar thicknesses that are adjustable along the span. The skin thicknesses are the same on the top and bottom and spar the same on the front and back. The front of the wingbox is at 10% chord, the rear is at 60% chord, and the shape is defined by a NASA SC2-0612 airfoil (adopted from Chauhan and Martins [33]). The mesh includes 28 aerodynamic panels across the span and 3 aerodynamic panels along the chord. The structural mesh uses the same discretization in the spanwise direction as the aerodynamic mesh. Table 2 lists the parameters used for the wing and wingbox. The weight of the wing structure is added as a distributed load in the finite element model, but no distributed fuel load is included. The model does not yet include a horizontal stabilizer to trim the aircraft. Nonetheless, OpenAeroStruct optimization results have been shown to closely match high-fidelity aerostructural optimizations even without including a horizontal stabilizer [33].

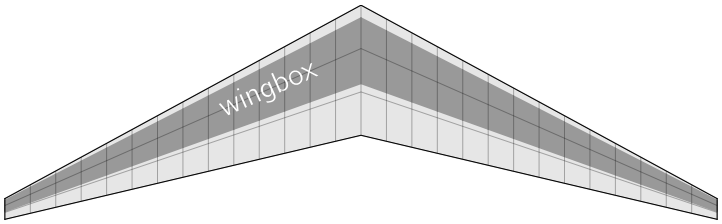

Figure 3: The baseline wing uses a simple planform with area, aspect ratio, taper, and sweep based on publicly available 737-800 data.

Airfoil shapes are not included in the optimization problem. The VLM formulation used to compute the induced drag assumes 2D panels, so it does not account for airfoil shapes. The viscous drag estimate uses a flat plate skin friction coefficient with a form factor correction. The Korn equation, which estimates wave drag, uses only the thickness-to-chord ratio. Because these aerodynamic models cannot account for detailed airfoil shapes, we exclude them as design variables. The impact of ignoring airfoil shape as a design variable is discussed at the end of Section 4. Note that the structural wingbox model does account for airfoil shape, which it uses to compute the area moments of inertia, torsion constant, and cross-sectional area. Varying the thickness-to-chord ratio scales the wingbox coordinates.

Parameter	Value
Planform area	124.6 m^2
Wingbox shape	10–60% chord of NACA SC2-0612 airfoil
Young's modulus	73.1 GPa
Shear modulus	27.5 GPa
Yield stress	420 MPa
Safety factor	1.5
Material density	2,780 kg/m^3

Table 2: Structural parameters are based on 7000-series aluminum used in the 737-800 wing.

2.3 Coupling of mission and aerostructural analyses

While OpenAeroStruct is fast, it is not fast enough to incorporate directly into OpenConcept's mission analysis. An OpenConcept mission uses somewhere on the order of 50 to 100 analysis points throughout the mission for numerical integration. The Newton solver converges this mission in roughly 5 iterations. If OpenAeroStruct were included directly, the aerostructural analysis and its derivative computation, which uses a combination of analytic and complex step methods, would be called hundreds of times. Secondly, if OpenAeroStruct is called directly, the Jacobian in the linear system of OpenMDAO's Newton solver would rapidly become unwieldy. Finally, this work may be used in OpenConcept optimizations that do not include wing design variables. In those cases, it would be beneficial to avoid the computational cost of repeatedly calling OpenAeroStruct within every optimization iteration. By using a surrogate, we call OpenAeroStruct only when the wing design changes and otherwise use the existing surrogate model.

These factors suggest that using a surrogate model would be a good solution. The OpenAeroStruct analyses required to train the surrogate model are quickly evaluated in parallel and need only be rerun when the wing design changes. This is also convenient for optimizations without wing design variables since the training data can be generated once at the beginning, and then the cheap surrogate can be used throughout.

While adding geometric parameters as inputs to the surrogate model may seem intuitive, it is not computationally tractable as the number of geometric design variables increases. Every additional input to the surrogate model adds a dimension to the required training data set. With potentially hundreds of geometric design variables, generating enough training data to create an accurate surrogate model in the high dimensional space is far too expensive.

The surrogate for this model uses SciPy's cubic interpolation [35]. It fits the surrogate quickly and is accurate for this application. If even more accuracy or fewer aerostructural analyses were necessary, kriging and other more advanced surrogate models could be considered [9, 23, 36]. The surrogate model is automatically retrained anytime the wing design changes, but will otherwise use existing data.

The inputs to the surrogate are Mach number, angle of attack, and altitude. Because all possible flight conditions of a mission must be captured, the surrogate is trained with Mach numbers from 0.1 to 0.9, angles of attack from -10 to 15 deg, and altitudes from 0 to 40,000 ft. Most training points are clustered between Mach 0.7 and 0.9 to capture the drag rise at high Mach numbers accurately. Overall, the surrogate performs a sweep over nine Mach numbers, six angles of attack, and four altitudes, resulting in 216 aerostructural analyses. These cases run in 40 seconds in parallel on a 16-core AMD Ryzen 5950X. The surrogate is accurate, estimating fuel burn to within tenths of a percent, so the training grid could be coarsened for further runtime improvements while still closely representing the OpenAeroStruct data.

2.4 Surrogate model accuracy

We compare two separate mission analyses to evaluate the surrogate model's accuracy. The first is a mission with the surrogate as the aerodynamic model. The second is a mission with OpenConcept calling OpenAeroStruct directly in the loop. Without a surrogate model, an OpenConcept mission analysis with OpenAeroStruct's aerostructural model incurs nearly a ten-fold increase in run time compared to a mission analysis with a surrogate model. This shows why an accurate surrogate is beneficial for mission analysis and optimization. When trained with 216 aerostructural analyses, the surrogate closely matches the mission run with OpenAeroStruct directly in the loop. Figure 4 shows the error due to the surrogate model in the 300 nmi mission and Figure 5 shows the same for the 2,900 nmi mission. The results match the exact values within a couple of tenths of a percent for both cases. An error this low indicates we could coarsen the 216 training points while maintaining sufficient accuracy. However, we can afford to have so many points because OpenAeroStruct is relatively cheap, and the training data generation is parallelized.

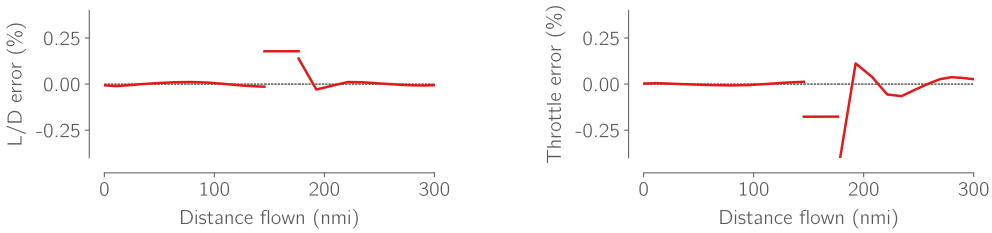

(a) Lift-to-drag ratio error in surrogate model

(b) Throttle error caused by L/D error

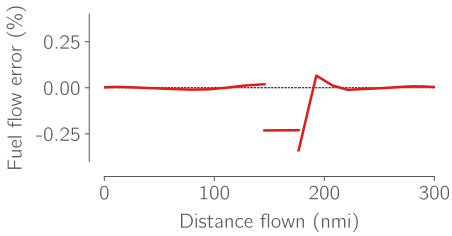

(c) Fuel flow error caused by throttle error

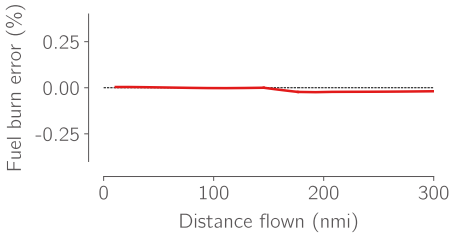

(d) Fuel burn error caused by fuel flow error

Figure 4: Mission analysis with the aerostructural surrogate estimates fuel burn to within 0.02% of the same mission run with OpenAeroStruct directly in the loop for the 300 nmi mission.

The flight conditions with the most significant errors are at high Mach numbers. This is due to the rapid increase in drag coefficient at high Mach numbers and high angles of attack, which can be seen in Figure 6. Since the 2,900 nmi mission spends more time in cruise ($M = 0.78$), the error accumulates and results in more fuel burn errors for the 2,900 nmi mission than the 300 nmi mission. The curvature is challenging for the surrogate model to capture, but it still performs well. More advanced surrogate modeling techniques, such as kriging models, could be used to better approximate this behavior.

For general purpose use within OpenConcept, estimating fuel burn to within tenths of a percent is more than sufficient. Suppose even more rapid evaluation is necessary, or the aircraft does not fly in the transonic regime. In that case, the grid of Mach numbers, angles of attack, and altitudes that is used to train the surrogate can be coarsened.

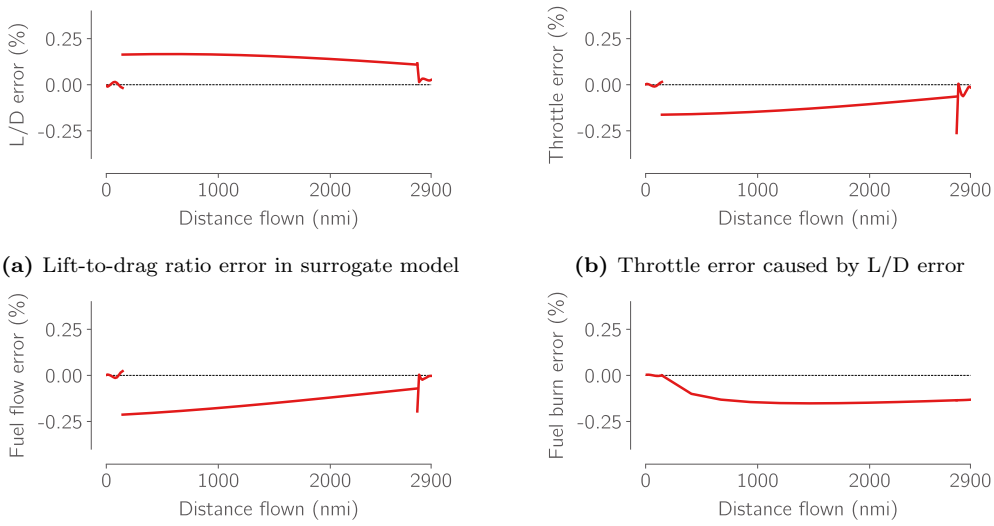

(a) Lift-to-drag ratio error in surrogate model

(b) Throttle error caused by L/D error

(c) Fuel flow error caused by throttle error

(d) Fuel burn error caused by fuel flow error

Figure 5: The 2,900 nmi mission with the surrogate model in the loop has slightly more error than the short one due to longer durations at high Mach numbers, but still estimates fuel burn to within 0.13% of the mission run with OpenAeroStruct called in the loop.

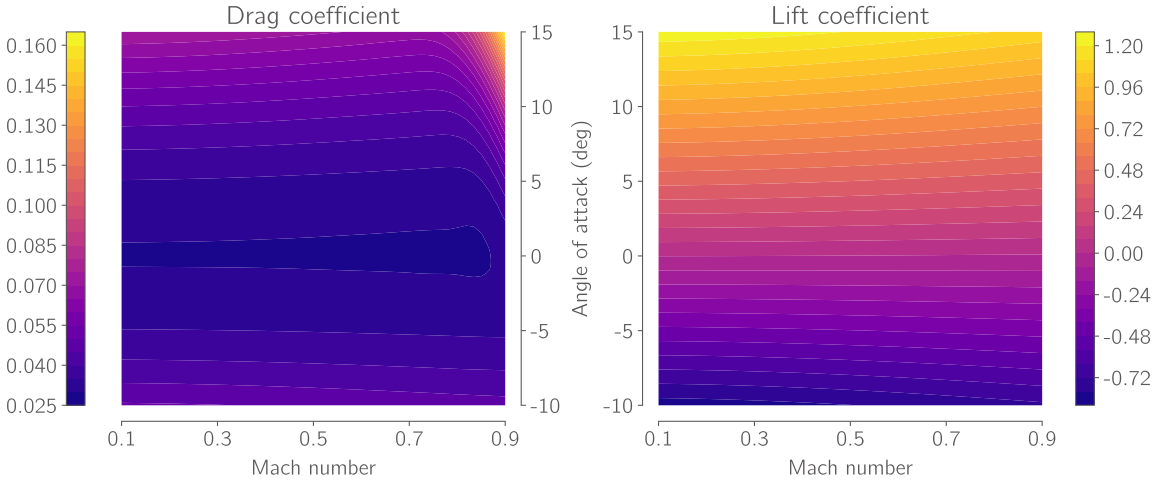

Figure 6: Drag and lift coefficient surrogate model at 30,000 ft.

2.5 Model validation

We validate the fuel burn value against estimated 737-800 values from other mission analysis tools, shown in Table 3. The validation mission has a range of 2,950 nmi, cruises at 35,000 ft and Mach 0.78, and carries 36,540 lbs of payload. The twist distribution of the 737-800's wing is not available, so we use one of the optimized designs for a fair comparison. We assume the wing is the one optimized by mission-based optimization at a range of 2,900 nmi. Our tool predicts a reasonable fuel burn value within roughly 10% of the other tools. The remaining differences may be due to assumptions in the engine model or variations in the climb and descent profiles.

Tool	Block fuel (lbs)
PASS	38,180
TASOPT	41,238
SUAVE	39,556
pyMission	38,687
This work	44,730

Table 3: Validation of 737-800 fuel burn against other tools (data from Kao et al. [37]).

3 Optimization

The mission-based optimization problem, listed in Table 4, is to minimize the fuel burn throughout the mission by varying the aerostructural wing design. Thanks to the modularity of OpenConcept, this could be easily extended to more complex models or other objective functions, such as the direct operating cost. To use a similar methodology as Kenway and Martins [4], we size the structure with a 2.5g maneuver condition at 20,000 ft, Mach 0.78, and maximum takeoff weight (MTOW). The angle of attack to satisfy lift equals weight at the maneuver condition is solved internally in OpenConcept using the Newton solver. The Kreisselmeier–Steinhauser function is used to aggregate the stress constraints of the wingbox [38, 39]. The aspect ratio is limited to 10.4 to meet the wingspan limit of the Group III gates used by the 737-800. The aspect ratio fully defines the wingspan because the wing area is held constant, so bounding the aspect ratio is equivalent to enforcing a span constraint. The thickness-to-chord ratio has a lower bound at 3%. The skin and spar thicknesses are assigned a lower bound of 3 mm, adopted from Chauhan and Martins [33]. We use a simple optimization problem formulation to gain intuition on the results from different objective functions. The optimized wings are not necessarily practical designs as they have only one load case and are missing other constraints, such as flutter and low-speed stall.

	Function/variable	Bound	Note	Qty
minimize	mission fuel burn		Computed by OpenConcept	
w.r.t.	aspect ratio	$\leq$10.4	Limited for Group III gate wingspan	1
	taper ratio			1
	quarter-chord sweep			1
	wing twist		B-spline interpolated, set to 0 deg at tip	3
	thickness-to-chord ratio	$\geq$3%	B-spline interpolated	4
	skin thickness	$\geq$3 mm	B-spline interpolated	4
	spar thickness	$\geq$3 mm	B-spline interpolated	4
			Total	**18**
subject to	von Mises stress at 2.5g	$\leq$280 MPa	20,000 ft and Mach 0.78 at MTOW	1
			Total	**1**

Table 4: The mission-based optimization problem uses a numerically integrated fuel burn as the objective function.

The goal is to compare the traditional single and multipoint methods to aerostructural optimization with the actual mission fuel burn as the objective function, mission-based optimization. To do this, we define the single and multipoint optimization problems to closely resemble the formulation used in previous high-fidelity single and multipoint aerostructural optimizations [2, 4].

Single-point optimization, listed in Table 5, estimates fuel burn based on a single aerostructural analysis in cruise. The fuel burn estimate uses the Bréguet range equation at the single-point flight condition with a constant thrust-specific fuel consumption value of 17.76 g/(kN-sec). The flight condition of the single-point is the cruise flight condition at Mach 0.78 and 35,000 ft, with half of the fuel burned. The initial weight is evaluated the same way as the mission-based weight by adding

to MTOW the difference between the new wing weight and original wing weight, as estimated by Raymer [32].

	Function/variable	Bound	Note	Qty
minimize	fuel burn		Computed with Bréguet range	
w.r.t.	aspect ratio	≤10.4	Limited for Group III gate wingspan	1
	taper ratio			1
	quarter-chord sweep			1
	wing twist		B-spline interpolated, set to 0 deg at tip	3
	thickness-to-chord ratio	≥3%	B-spline interpolated	4
	skin thickness	≥3 mm	B-spline interpolated	4
	spar thickness	≥3 mm	B-spline interpolated	4
	cruise angle of attack			1
	maneuver angle of attack			1
			Total	**20**
subject to	von Mises stress at 2.5g	≤280 MPa	20,000 ft and Mach 0.78 at MTOW	1
	cruise $L = W$		Weight with half of fuel burned	1
	maneuver $L = W$		MTOW at 2.5g	1
			Total	**3**

Table 5: The single-point optimization problem computes the fuel burn objective function using a single aerostructural analysis in cruise and the Bréguet range equation.

Multipoint optimization, listed in Table 6, is intended to avoid the single-point formulation's pitfall of improving on-design performance at the cost of worse off-design performance. Kenway and Martins [40] show the improved performance of multipoint aerodynamic shape optimization over single-point across a range of operating conditions. Liem et al. [23] report a similar conclusion for aerostructural optimization. This multipoint implementation uses the same approach as Kenway and Martins [4], where the design cruise condition is perturbed by Mach 0.01 and 1,000 ft in altitude. This results in five flight conditions, shown in Figure 7. To compute the objective function, the fuel burn estimates use the same method as the single-point for each flight condition. The average of the five fuel burns becomes the objective.

	Function/variable	Bound	Note	Qty
minimize	fuel burn		Average of five cruise conditions	
w.r.t.	aspect ratio	≤10.4	Limited for Group III gate wingspan	1
	taper ratio			1
	quarter-chord sweep			1
	wing twist		B-spline interpolated, set to 0 deg at tip	3
	thickness-to-chord ratio	≥3%	B-spline interpolated	4
	skin thickness	≥3 mm	B-spline interpolated	4
	spar thickness	≥3 mm	B-spline interpolated	4
	cruise angles of attack			5
	maneuver angle of attack			1
			Total	**24**
subject to	von Mises stress at 2.5g	≤280 MPa	20,000 ft and Mach 0.78 at MTOW	1
	cruise $L = W$		Weights with half of fuel burned	5
	maneuver $L = W$		MTOW at 2.5g	1
			Total	**7**

Table 6: The multipoint problem's objective averages fuel burns from five different cruise conditions. The fuel burn for each cruise condition is computed the same way as is done for the single-point problem.

To fairly compare the optimization methods, the resulting wing design from each optimization method is run on the mission profile in OpenConcept by calling OpenAeroStruct directly instead of using the surrogate.

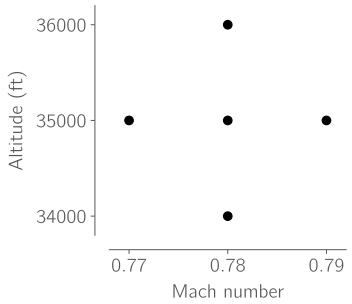

Figure 7: Multipoint averages fuel burn estimates from five flight conditions for its objective function.

4 Discussion

The hypothesized pitfall of traditional aerostructural optimization methods is that the Bréguet range fuel burn model poorly estimates the total mission fuel burn as the cruise fuel burn becomes less dominant. This is because all analyses are performed for cruise conditions, so the performance in the climb is not modeled. Thus, as the cruise segment becomes shorter, the optimizer will design a wing to minimize a fuel burn approximation that inaccurately reflects the actual fuel burn. To investigate this hypothesis, we run aerostructural optimizations with the three optimization methods on missions ranging from 300 nmi to 2,900 nmi. On the 300 nmi mission, the cruise segment is only 31 nmi and makes up a small fraction of the fuel burn. On the 2,900 nmi mission, the cruise segment is over 2600 nmi and dominates the fuel burn.

All optimizations reduce the optimality by at least 3–4 orders of magnitude and achieve a feasibility of 10^{-6}, as defined by SNOPT [41]. The single-point cases take roughly 5 min on a single thread. The multipoint optimizations run for 20-30 min on a single thread. The mission-based optimizations require 90 min to reach the same optimality while running the aerostructural analyses to train in parallel using all 32 threads of the AMD Ryzen 5950X.

The results from the three optimization methods on the range of mission lengths are shown in Figure 8; data for three cases are listed in Appendix A. The most significant difference in actual fuel burn between the three optimized wings is only 1.3%. However, there is an evident trend as the mission range decreases. Because the mission-based optimization is designing the wing using the most accurate model of mission fuel burn, it always finds a better wing design than single-point and multipoint. This effect is especially noticeable for short missions where the mission-based optimization can properly trade off the wing's low and high-speed performance in the different flight segments. Multipoint optimization improves over a single-point formulation as the mission range decreases, but the effect is much less pronounced than mission-based optimization. Even for missions at the top end of the 737's range, mission-based optimization finds a better design, though only tenths of a percent better. This is partially because the mission-based optimization considers climb, which offers information about the effect of the lower-speed performance in climb and structural weight on mission fuel burn. The fuel burn savings in long missions are also because mission-based optimization can account for variations in the angle of attack during cruise. Mission-based optimization computes fuel burn by integrating fuel flow across the mission, which means that the lift-to-drag ratio at every numerical integration point affects the fuel burn. This incentivizes the optimizer in the mission-based problem to improve performance across all flight conditions in the mission, as opposed to the small number of flight conditions in the single and multipoint problems. The variation in the angle of attack is because the mission profile maintains the same altitude and Mach number for the entire duration of cruise, shown in Figure 9. In reality, a stepped climb would be used during cruise to maintain a more constant angle of attack.

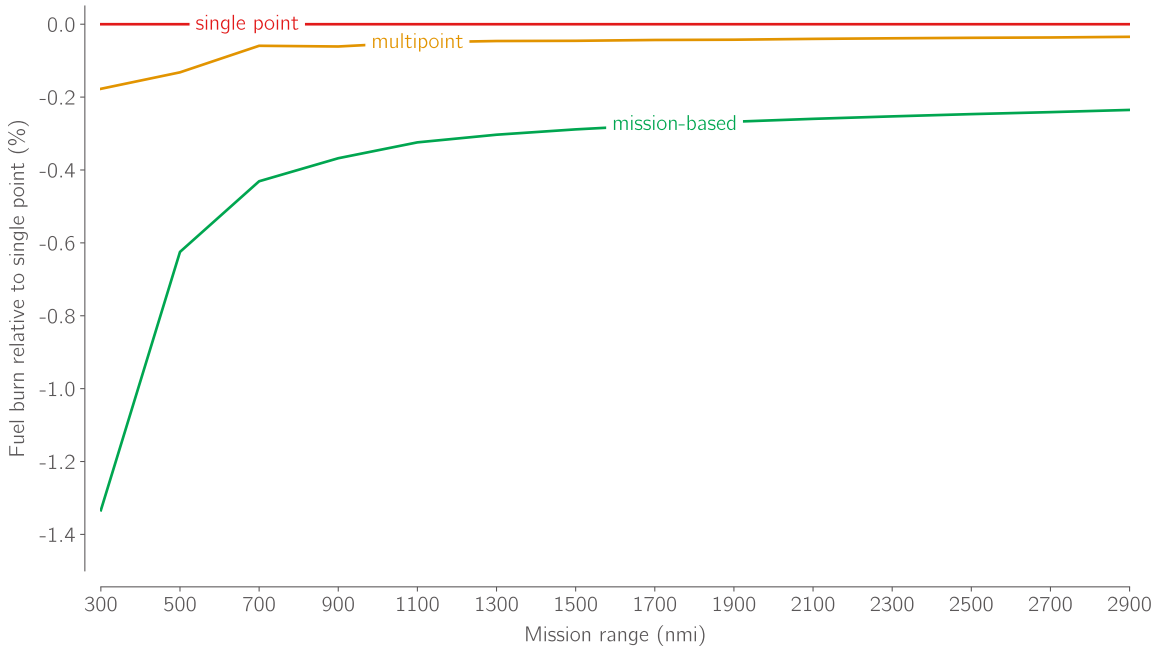

Figure 8: Mission-based optimization outperforms other conventional methods, particularly for short missions.

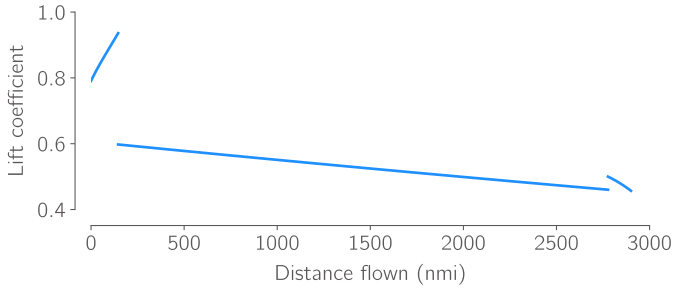

Figure 9: On long missions, the lift coefficient varies slightly throughout cruise as fuel is burned.

By inspecting the relative fuel burn in the mission segments for the mission-based optimized designs, shown in Figure 10, we can understand the reason for the difference in fuel burn among the optimization methods. The figure shows that considering performance in the climb, and generally in flight segments other than cruise, is essential for shorter missions because climb fuel burn can make up half, or more, of the total fuel burn. The traditional aerostructural optimization approaches are unaware of these trends, so they miss out on the benefits.

By comparing the wing design, we can further explain the different decisions made by the optimizers for the three optimization problems. Figure 11 shows the thickness-to-chord ratio and structural thicknesses for wings optimized with the three different methods on the shortest and longest missions. The thickness-to-chord ratios at the tip are on the low side for transport aircraft. As mentioned in Section 3, we give the optimizer freedom so we can more clearly compare the behavior with different objectives. This may result in designs that do not satisfy all practical constraints. The mission-based optimization identifies that the fuel burn in the climb during the 300 nmi mission is much more substantial than the fuel burn during cruise. It uses this knowledge to better optimize the wing for the lower speeds in climb, rather than shaping the wing for the high-speed cruise. This manifests as a greater thickness-to-chord ratio than the single-point and

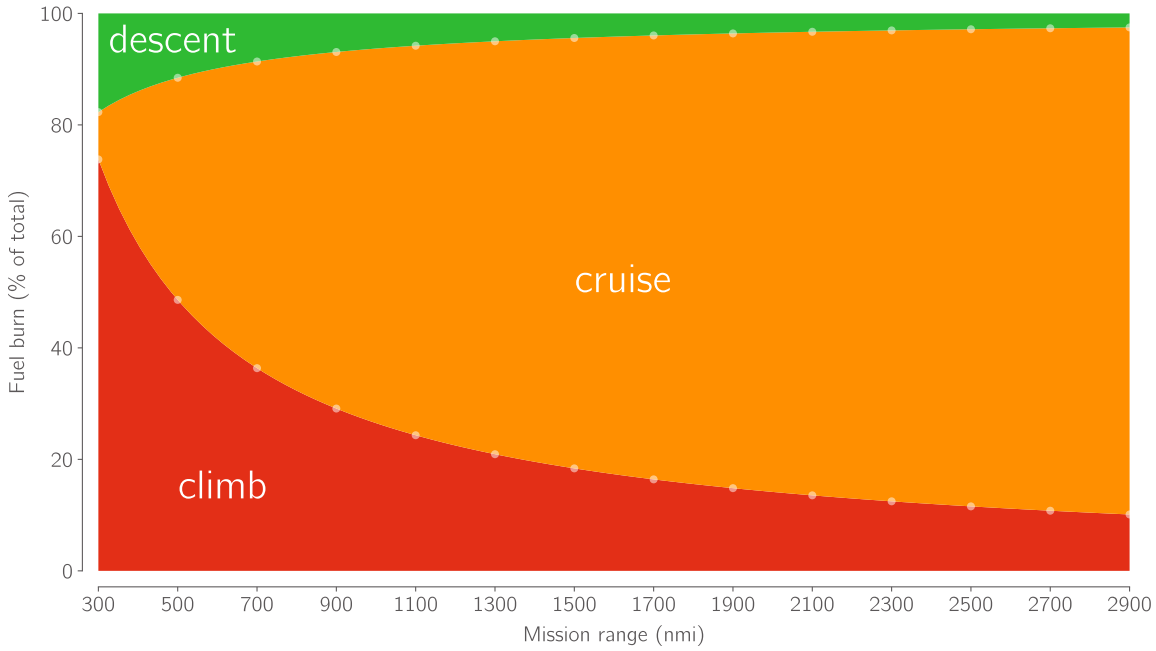

Figure 10: Fuel burn in climb exceeds cruise fuel burn for shorter missions.

multipoint cases, allowing it to reduce the wingbox weight using thinner spars and skins. On the 2,900 nmi mission, the thickness-to-chord distributions are nearly identical between the three designs. This is because high-speed performance becomes most important when the cruise segment dominates. It is no longer beneficial to reduce weight by increasing the thickness-to-chord ratio, which increases wave drag.

The optimized planform shapes from the three objective functions are shown in Figure 12 for the shortest and longest missions. All designs fall on the upper bound of the span limit, which is enforced via an upper bound on aspect ratio. On the 300 nmi mission, mission-based optimization reduces the sweep compared to the other objectives' designs. The reduced sweep increases wave drag in cruise but allows for a lighter structure, which is a worthwhile tradeoff for the short mission. It is not a beneficial tradeoff for the long mission, so the planform shapes from the three objectives are similar.

Mission-based optimization shifts the lift slightly inboard at the 2.5g structural sizing condition, shown in Figure 13, further enabling a lighter wingbox structure. These results show that the thickness-to-chord ratio is a critical aerostructural design variable because it affects aerodynamic and structural performance. A smaller thickness-to-chord ratio results in a wing with lower wave drag at the cost of increased weight since it needs a heavier structure to support the bending loads.

Due to the increased thickness-to-chord ratio, the mission-based optimization arrives at a much lighter optimized wing design across all mission ranges. This is a significant result because an aircraft's weight is closely related to its purchase price [42]. Takeoff gross weight has been used as an objective function for aerostructural optimization because of its relationship to both acquisition cost and fuel burn [4, 43].

Figure 14 shows that mission-based optimization returns a wing up to 25% lighter than the wing from the two traditional optimization approaches. One reason is that mission-based optimization can consider the impact of weight on thrust, and thus on fuel burn, when the flight path angle is not zero. The Bréguet range equation assumes that lift equals weight and thrust equals drag. This is not true when the aircraft is climbing or descending since a component of weight acts along the

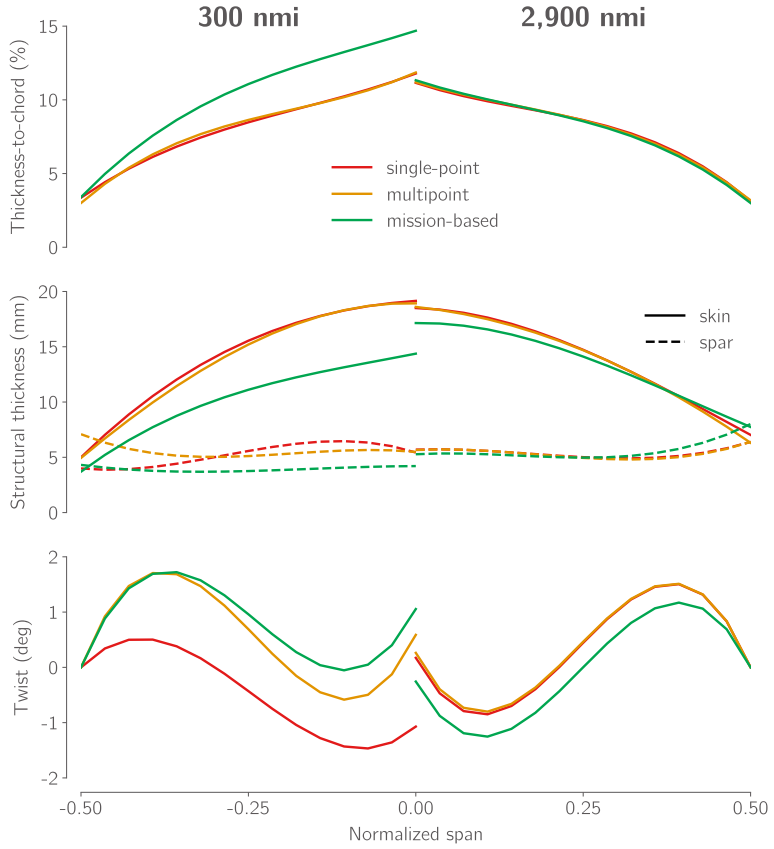

Figure 11: For the 300 nmi mission, mission-based optimization reduces fuel burn compared to single-point and multipoint by increasing the thickness-to-chord ratio, enabling a lighter structure. The designs are more similar on the longer 2,900 nmi mission.

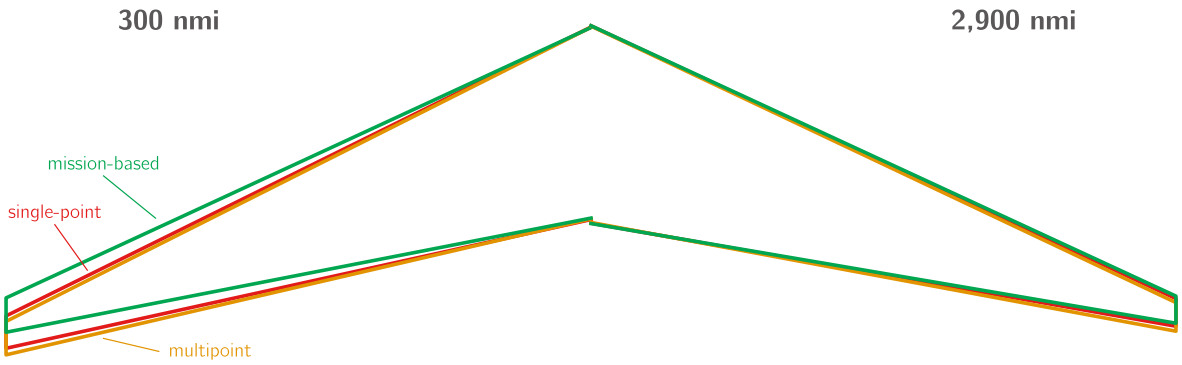

Figure 12: On the short mission, mission-based optimization converges to a lower sweep than single-point and multipoint, which helps reduces structural weight. On the long mission, the planform designs are very similar.

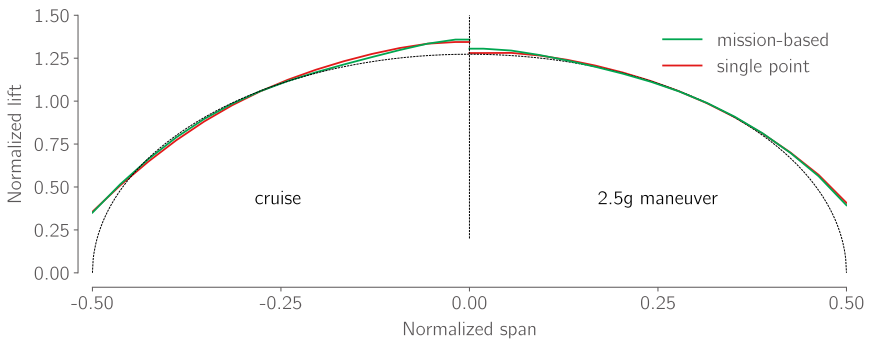

Figure 13: On the 300 nmi mission, mission-based optimization shifts the lift slightly inboard at the 2.5g sizing condition to decrease the bending moment at the root, further reducing the required structural weight.

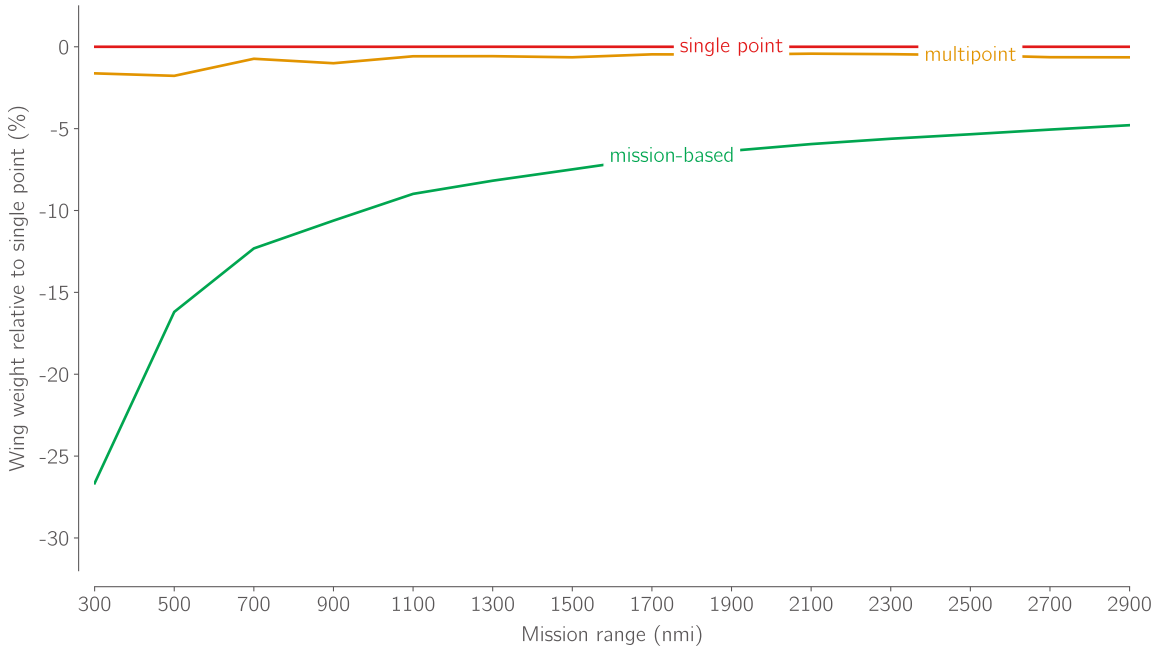

Figure 14: The wing is much lighter with mission-based optimization than single-point or multipoint.

same axis as the thrust. OpenConcept's mission analysis captures this effect. Thus, it is in the interest of mission-based optimization to decrease the weight to reduce the climb fuel burn.

On the shorter missions, mission-based optimization sacrifices aerodynamic efficiency in cruise to achieve weight savings, as shown in Figure 15. Surprisingly, the optimizer finds that over a 4% decrease in the lift-to-drag ratio in cruise is worthwhile to decrease climb fuel burn by reducing wing weight. The lift-to-drag ratios are taken from the middle numerical integration point in the cruise segment.

Generalizing these results to RANS-based optimizations, we expect the fuel burn difference between traditional and mission-based approaches to grow slightly. RANS can predict the effect of small changes to the wing's airfoil shapes that OpenAeroStruct cannot. Accordingly, RANS-based optimizations tend to use more shape design variables and thus specialize the design to certain flight conditions more than OpenAeroStruct. This specialization often degrades off-design performance, particularly for the single-point optimization, which could increase actual mission fuel burn. For example, including airfoil shape in a single-point design would likely guide the optimizer toward

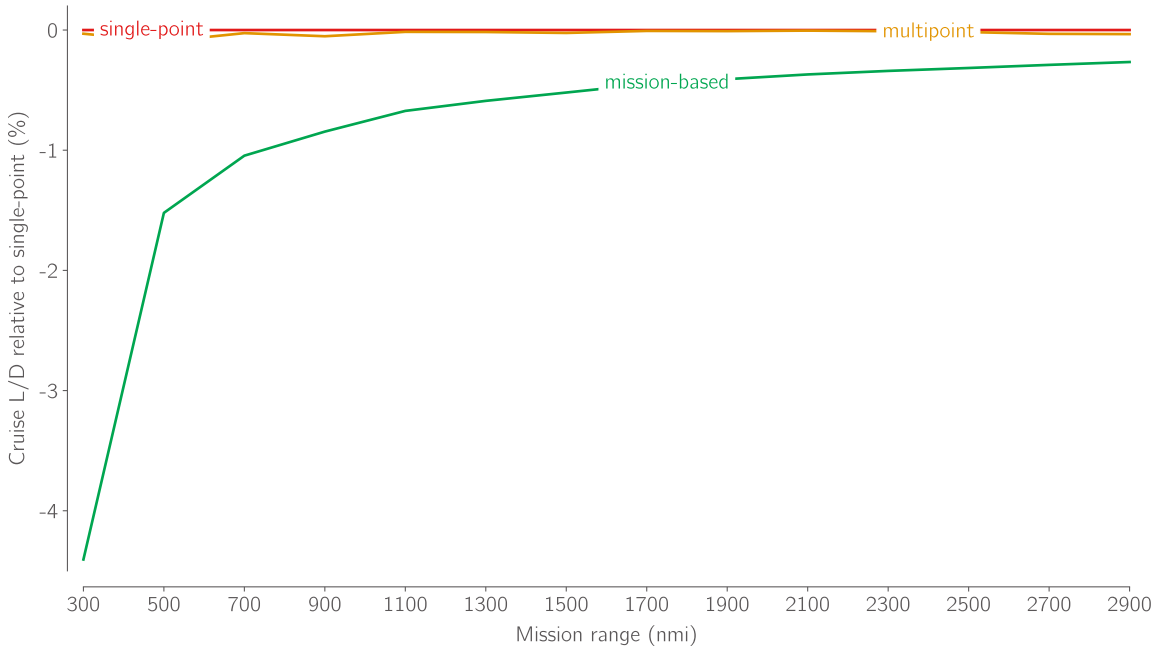

Figure 15: Mission-based optimization sacrifices drag in cruise to decrease weight, reducing overall fuel burn.

supercritical airfoil shapes. Adding climb information would allow it to balance wave drag reduction with supercritical airfoils against airfoil shapes that increase efficiency at lower speeds. These effects slightly expand the set of missions for which it is essential to consider climb performance in the objective function (Section 5 proposes an easy way to do this).

5 Sequential Bréguet range: a low-cost improvement for high-fidelity optimizations

Motivated by the substantial fuel burn in the climb segment shown in Figure 10 and single-point and multipoint's poor modeling of the climb, we propose a modification to the traditional fuel burn objective. This approach attempts to gain the fuel burn and wing weight improvements of mission-based optimization without the complexity and cost of adding a surrogate and numerically simulating the mission. We first derive a modified version of the Bréguet range equation that incorporates the effects of nonzero flight path angles, such as for climb and descent. Instead of modeling the mission with a single evaluation of this equation, like single-point and multipoint formulations, this new objective uses two or more sequential evaluations. For this case, we use a single aerostructural analysis in climb and a single one in cruise. Though it could be included, we ignore fuel burn in descent since it is small compared to climb and cruise fuel burn (as seen in Figure 10) and would require an additional aerostructural analysis. This approach can model arbitrarily complicated mission profiles, such as a step climb, by adding more sequential evaluations of the fuel burn equation.

5.1 Derivation

The Bréguet range equation assumes lift equals weight and thrust equals drag. While this is a reasonable assumption when flying level, it ignores crucial effects when the flight path angle is

nonzero. In climb and descent, weight is decomposed in the steady force balance as

$$L = W\cos\gamma \tag{1}$$
$$T = D + W\sin\gamma \tag{2}$$

where γ is the flight path angle (positive is climb). By incorporating these assumptions into the range equation derivation, we find the climb and descent range equation:

$$R = \frac{1}{\frac{\cos\gamma}{\frac{L}{D}} + \sin\gamma}\frac{V}{\text{TSFC}}\ln\frac{W_i}{W_f} \tag{3}$$

When the flight path angle is zero, this reduces to the standard Bréguet range equation. This equation has also been derived for modeling fuel burn in a cruise-climb by Hale [44]. A similar equation is presented by Raymer [32] (Equation 17.94) but is in a form that does not retrieve the original Bréguet range equation when the climb angle is zero.

The assumptions of constant lift-to-drag ratio and thrust-specific fuel consumption are less reasonable for climb and descent, where the flight conditions vary. However, the equation still substantially improves the original fuel burn approximation. Since commercial aircraft climb angles are 2–4 degrees, the small angle approximation can be used here. Fuel burn is computed by manipulating Equation 4 to solve for $W_i - W_f$. The result is

$$\text{fuel burn} = W_i - W_f = W_i\left\{1 - \exp\left[-\left(\frac{1}{\frac{L}{D}} + \gamma\right)\text{TSFC}\frac{R}{V}\right]\right\} \tag{4}$$

5.2 Computation procedure

The procedure used to compute the fuel burn at the end of the cruise segment is the following:

1. Perform an aerostructural analysis at the flight condition halfway through the climb.
2. Use Equation 4 to compute the fuel burn in climb. The initial weight, W_i, is the takeoff weight and the range, R, is the length of the climb segment as defined by the mission profile. The flight path angle, γ, is taken to be $\tan^{-1}(h_{\text{cruise}}/R_{\text{climb}})$, which assumes a constant flight path angle throughout climb.
3. Perform an aerostructural analysis halfway through the cruise segment.
4. Use Equation 4 to compute fuel burn in cruise. W_i for this cruise segment calculation is the final weight, W_f, from the climb fuel burn calculation (takeoff weight minus climb fuel burn). R is the cruise length as defined by the mission profile. In this case $\gamma = 0$, so the equation reduces to the standard Bréguet range equation.
5. Compute the objective function as the sum of the fuel burns from the climb and cruise segments. This can also be computed as the initial climb weight minus the final cruise weight.

The midpoint of each flight segment is used as the analysis point to follow the precedent set in [4]. In this work, the midpoint flight condition is defined by the Mach number and altitude of each flight segment's middle numerical integration point in the mission analysis. This information may not be available in all cases, so we suggest using the climb flight speed and half of the cruise altitude to define the midpoint flight condition in the climb. This fuel burn computation is only an

approximation because it assumes that the product of L/D, $TSFC$, and V is constant in climb, which is likely not the case on a real mission. Thus, it is not critical that the flight condition is precisely at the halfway point.

The optimizer determines the angles of attack to satisfy lift equals weight for the two aerostructural analyses. This is the same way as is done in the single-point and multipoint problems listed in Tables 5 and 6. The climb analysis assumes that half of the fuel weight computed in step 2 has been burned. The cruise analysis assumes the climb fuel and half of the cruise fuel have been burned. The optimization problem listed in Table 7 is similar to the single-point optimization problem but with a new objective function calculation and associated design variables and constraints for the climb.

	Function/variable	Bound	Note	Qty
minimize	climb plus cruise fuel burn		Sequential evaluations of Equation 4	
w.r.t.	aspect ratio	≤10.4	Limited for Group III gate wingspan	1
	taper ratio			1
	quarter-chord sweep			1
	wing twist		B-spline interpolated, set to 0 deg at tip	3
	thickness-to-chord ratio	≥3%	B-spline interpolated	4
	skin thickness	≥3 mm	B-spline interpolated	4
	spar thickness	≥3 mm	B-spline interpolated	4
	climb angle of attack			1
	cruise angle of attack			1
	maneuver angle of attack			1
			Total	**21**
subject to	von Mises stress at 2.5g	≤280 MPa	20,000 ft and $M = 0.78$ at MTOW	1
	climb $L = W$		Weight with half of climb fuel burned	1
	cruise $L = W$		Weight with climb and half cruise fuel burned	1
	maneuver $L = W$		MTOW at 2.5g	1
			Total	**4**

Table 7: The improvement to the traditional aerostructural problems uses sequential evaluations of the modified Bréguet range equation (Equation 4) for climb and cruise.

Figure 16 shows how the necessary components are connected to compute the objective and constraints required by the optimizer. All aerostructural analyses can be run in parallel because they rely only on updated design variable information from the optimizer. Note how the amount of fuel burned during climb does affect the lift required in cruise. The optimizer solves this relationship using the cruise $L = W$ constraint.

This approach can incorporate a multipoint cruise segment or a mission profile with more segments. For example, a multipoint cruise could be included using the same calculation for climb fuel burn but then average the cruise fuel burn (steps 3 and 4) from a handful of different cruise flight conditions.

5.3 Discussion

We revisit the same plots as before to assess the benefit of using this approach but now with the new objective's designs. Figure 17 shows the fuel burn of the four objective functions relative to the single-point optimization. The new objective function that includes a climb analysis performs better than single-point and multipoint. It finds a much better design for the shorter missions than single-point and multipoint, which ignore performance in the climb.

The proposed objective function achieves similar wing weight reduction to mission-based optimization. Figure 18 shows that the new objective yields a lighter wing for shorter missions than mission-based optimization. These weight savings are because the single-point + climb objective

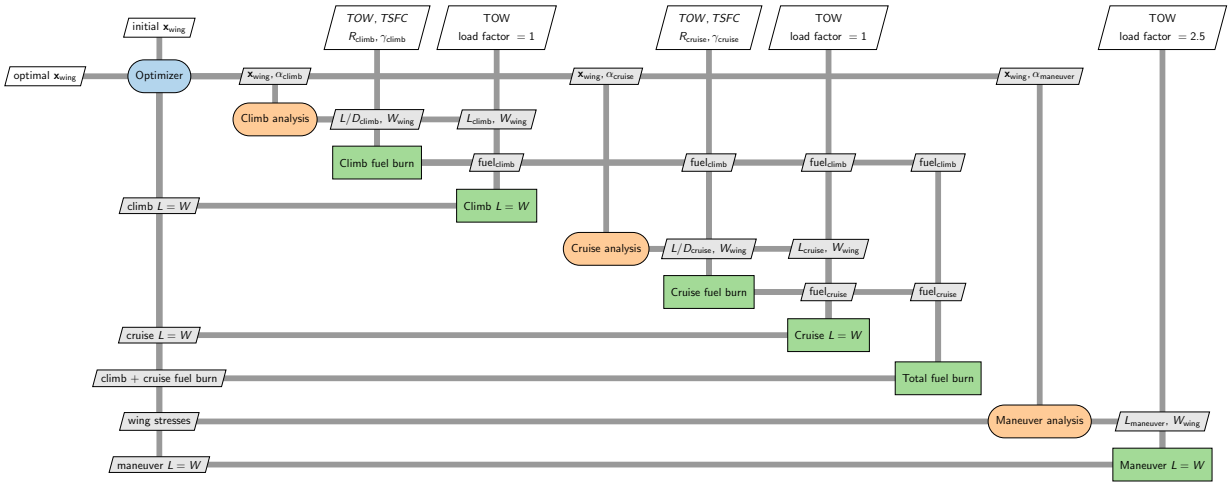

Figure 16: XDSM [30] showing the model setup for the sequential Bréguet optimization problem. The setup allows the three aerostructural analyses to be run in parallel.

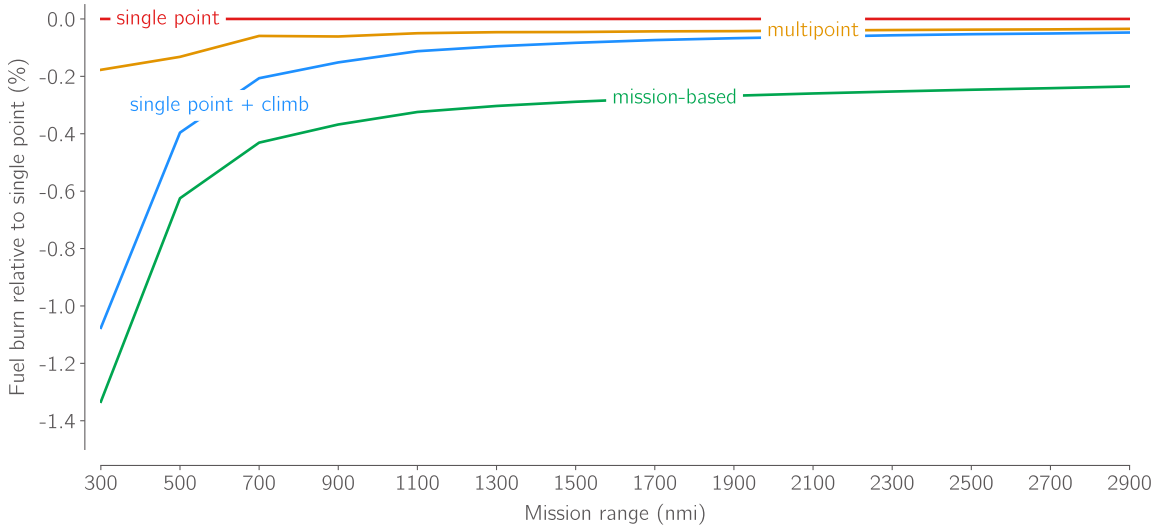

Figure 17: Including the climb fuel burn separately in the optimization offers significant improvements over single-point and multipoint, especially for short missions.

slightly overpredicts climb fuel burn, which puts an even greater emphasis on weight savings than in the mission-based optimization.

Figures 19 and 20 show that the single-point + climb objective returns a wing that is much closer in design to the wing designed with mission-based optimization. The single-point + climb design has a slightly higher thickness-to-chord ratio and slightly lower structural thickness than the mission-based design due to overprediction of climb fuel burn. This shows that the new objective gives the optimizer enough information to properly trade-off climb and cruise performance, despite the simplifications.

Until now, all fuel burn values we have shown come from taking the designs optimized with each objective and running them in OpenConcept. However, it is interesting to see how closely the fuel burn approximations, the objective functions, match the value computed by OpenConcept for a given wing design. Figure 21 shows the fuel burn estimated by each approximation relative to

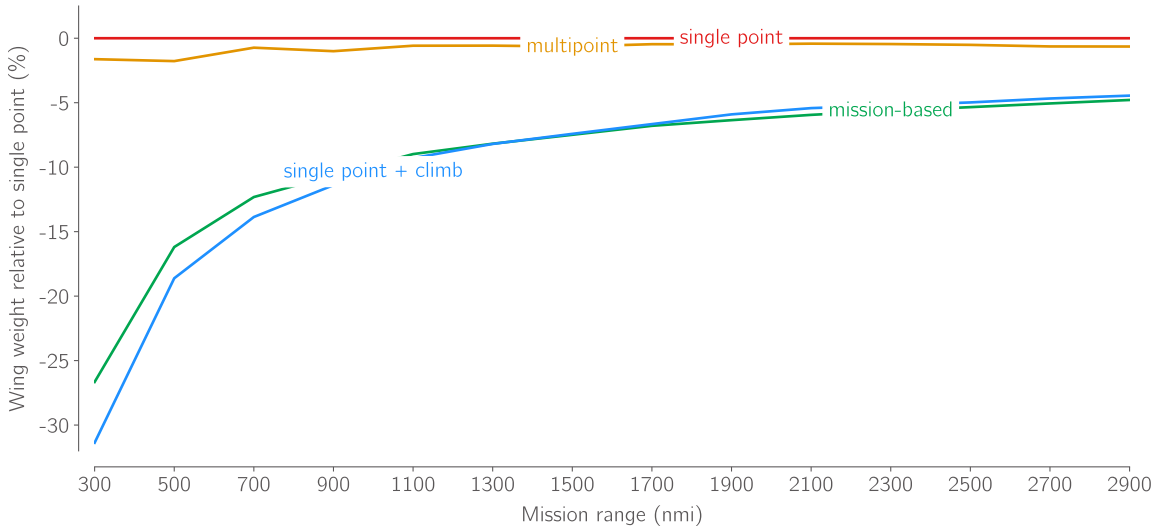

Figure 18: The proposed objective function achieves similar wing weight benefits to mission-based optimization, significantly outperforming both traditional optimization methods.

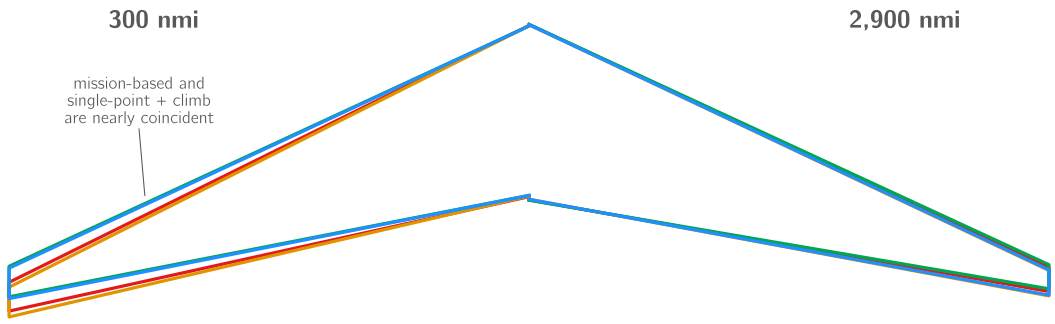

Figure 19: The planform geometries from the mission-based and single-point + climb optimizations are nearly identical for the 300 nmi mission. On the longer mission, all planform shapes are similar.

the actual fuel burn computed by OpenConcept. The sequential Bréguet estimate has half as much error in the fuel burn as the conventional Bréguet range estimate relative to full mission analysis. The constant error across all mission ranges is due to the error in Bréguet range's estimate of the cruise fuel burn and is attributed to the variation in the cruise flight condition for longer missions, shown in Figure 9.

Finally, we compare the computation time required for each type of optimization. The cases were run on an AMD Ryzen 5950X. All optimizations are run on a single processor, except for generating the training data for the mission-based surrogate model, which uses all available processors. These optimizations achieve the same optimality and feasibility tolerances as the previous optimizations.

The wall time for each optimization is shown in Figure 22. The single-point cases finish in 5–10 min, the multipoint cases in 20–30 min, the mission-based cases in 60–80 min, and the new objective cases in 10–20 min. The new objective achieves results with performance near the mission-based results, but in a quarter of the time.

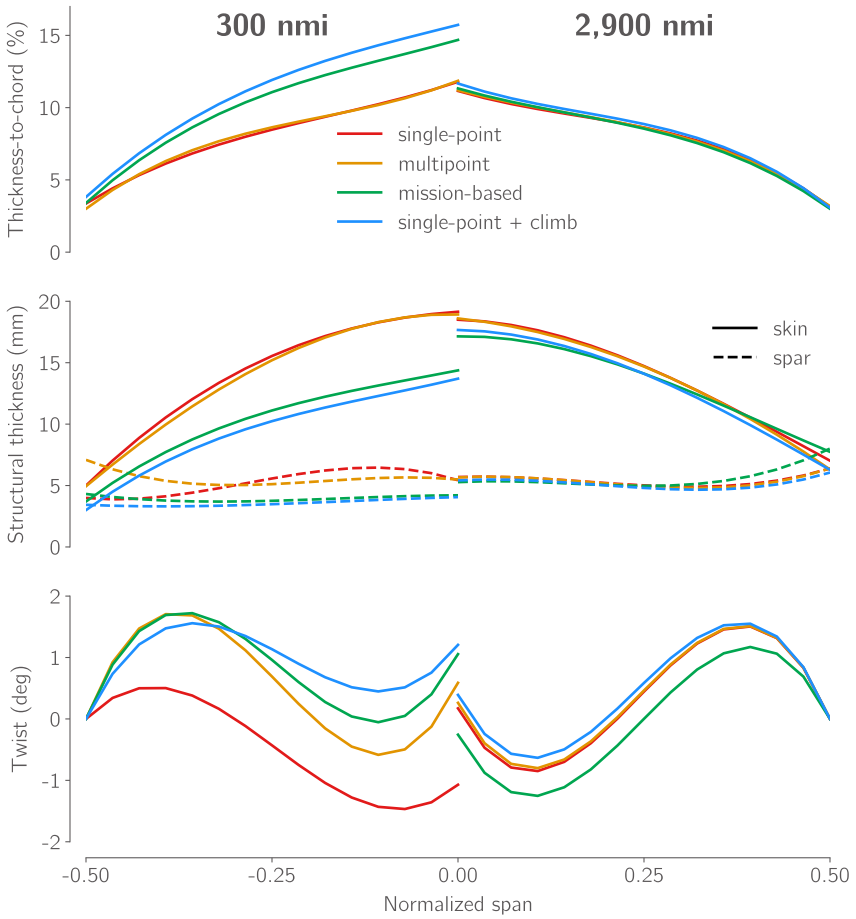

Figure 20: The new objective achieves a design with thickness-to-chord and structural thickness distributions that are much closer to the mission-based optimization design than to the designs from traditional objectives.

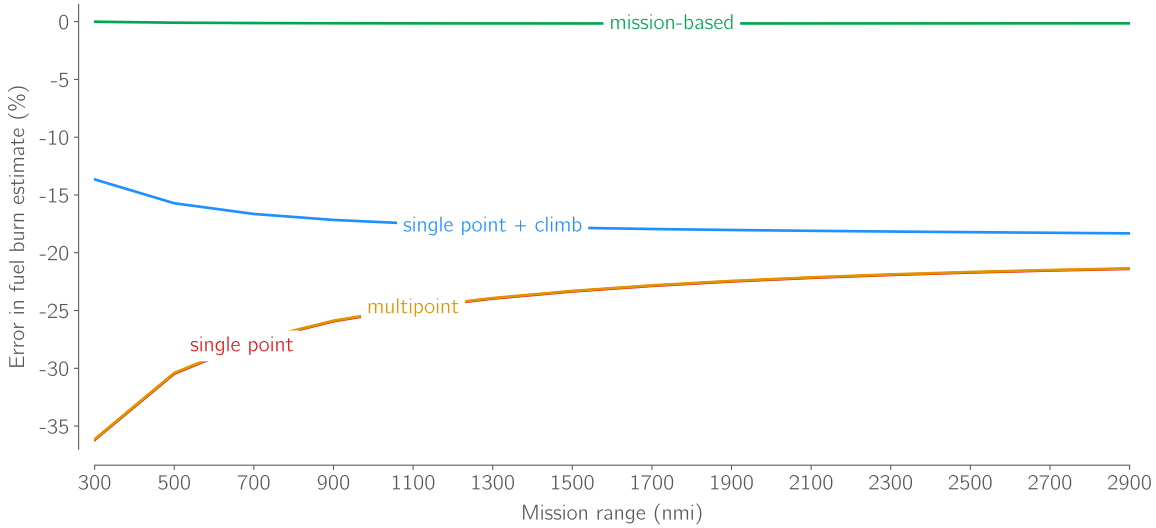

Figure 21: The new method better approximates the actual fuel burn compared to single-point. For this figure, a fuel burn estimation in descent for single-point + climb is included for a fair comparison between the methods.

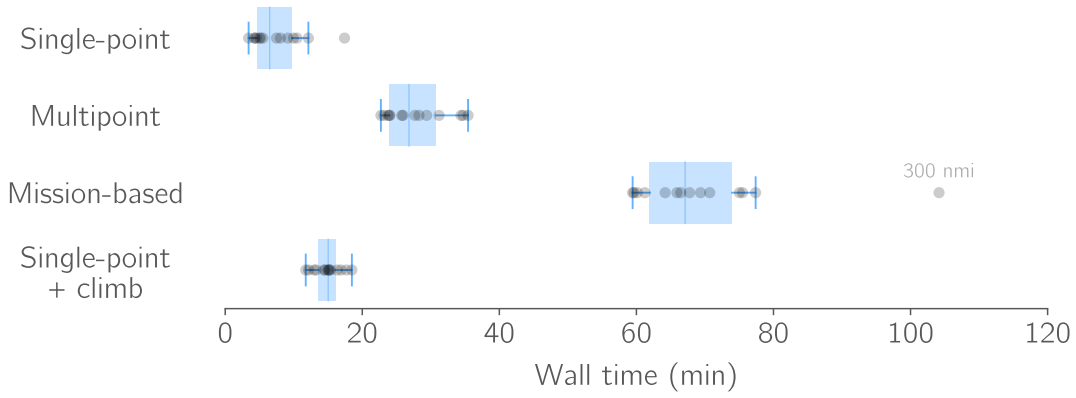

Figure 22: The new objective enables the optimizer to find wing designs similar to mission-based optimizations, but in a quarter of the time.

6 Conclusions

In this work, we show that traditional single-point and multipoint aerostructural optimization methods realize most of the fuel burn improvement compared to an approach that uses a more accurate fuel burn objective—within 1–2% of each other. This holds even for extreme cases where climb fuel burn makes up most of the total fuel burn. These results are found by analyzing a Boeing 737-sized airplane on mission ranges from 300 to 2,900 nmi. As the mission range increases, the wings designed by the different objective functions converge toward the same fuel burn value. The convergence of optimized designs as the mission range increases is a promising sign for single and multipoint optimizations. It indicates that, particularly for long-range aircraft, the fuel burns of designs optimized with traditional approaches match the optimum based on a true mission-based fuel burn objective within fractions of a percent.

The mission-based optimization, which computes climb fuel burn, returns a wing up to 25% lighter than the wings from single and multipoint optimizations. These findings show that while performance between the optimization methods may be similar as measured by the objective function, other essential design aspects vary considerably. Mission-based optimization arrives at a similar fuel burn objective function value as single-point and multipoint optimizations. However, the design it uses to achieve that fuel burn is different.

To bridge this gap, we present an improved aerostructural optimization objective that achieves most mission-based optimization's benefits, both in fuel burn and wing weight, by considering the climb segment more accurately. It uses a modified Bréguet fuel burn estimate that models nonzero flight path angles. The estimate is evaluated sequentially for each flight segment—climb and cruise in this case—and uses cumulative fuel burn from previous segments to determine the weight for the following segments. This approach requires similar computational resources to traditional methods and minimal additional implementation for existing high-fidelity codes, unlike mission-based optimization. Aerostructural optimizations with the improved objective function return designs that closely resemble those optimized with the mission-based objective. The single-point + climb objective also performs similarly to the mission-based objective. It obtains the majority of the fuel burn savings and greater wing weight reductions than the mission-based optimization. This new approach is flexible in that it can model arbitrary mission profiles by customizing the number of individual fuel burn segments and flight conditions. For example, this approach could be used to more accurately model a step climb in cruise or unconventional mission profiles for high-fidelity optimization.

In the future, these concepts can be applied to high-fidelity aerostructural optimizations to produce designs with even better real-world performance. Further practical constraints, such as for flutter or high lift performance, can be added to continue pushing the boundaries of what is possible with aerostructural optimization.

A Appendix

Table 8 contains optimization result data for the 300, 1500, and 2,900 nmi missions. The spline control points for the twist, thickness-to-chord, spar thickness, and skin thickness design variables are ordered from values at the tip of the wing to the root. The twist control point at the tip is locked at 0 deg to prevent rigid body motion. The arrays in the multipoint cruise angle of attack and cruise $L = W$ rows are ordered as follows:

1. Mach 0.78, 35,000 ft
2. Mach 0.79, 35,000 ft
3. Mach 0.77, 35,000 ft
4. Mach 0.78, 34,000 ft
5. Mach 0.78, 36,000 ft

		Unit	Lower	Upper	Single-point	Multipoint	Mission-based	Single-point + climb
minimize	mission fuel burn	kg			2,770.44	2,765.53	2,733.49	2,740.63
w.r.t.	aspect ratio			10.401	**10.401**	**10.401**	**10.401**	**10.401**
	taper ratio				0.168	0.174	0.180	0.180
	sweep	deg			23.046	23.524	21.577	21.754
	twist	deg			[0.000, 2.072, -2.862, -1.072]	[0.000, 5.274, -3.630, 0.588]	[0.000, 4.997, -2.787, 1.055]	[0.000, 4.084, -1.460, 1.206]
	t/c ratio		0.030		[0.034, 0.086, 0.090, 0.118]	[**0.030**, 0.096, 0.085, 0.119]	[0.034, 0.112, 0.123, 0.147]	[0.038, 0.117, 0.136, 0.157]
	spar thickness	mm	3.000		[3.990, **3.000**, 8.722, 5.434]	[7.088, **3.000**, 6.438, 5.490]	[4.313, **3.000**, 4.177, 4.206]	[3.431, **3.000**, 3.788, 4.058]
	skin thickness	mm	3.000		[4.997, 14.940, 18.469, 19.150]	[4.943, 13.349, 19.230, 18.926]	[3.701, 11.204, 12.398, 14.375]	[**3.000**, 10.435, 11.306, 13.701]
	maneuver AoA	deg			11.915	10.445	—	8.866
	cruise AoA	deg			8.76	[7.72, 7.54, 7.91, 7.38, 8.07]	—	6.44
	climb AoA	deg			—	—	—	9.493
subject to	2.5g failure			0.000	2.8×10^{-6}	1.3×10^{-7}	9.1×10^{-8}	6.2×10^{-8}
	maneuver $L = W$		0.000	0.000	1.8×10^{-8}	-4.4×10^{-9}	—	-4.4×10^{-10}
	cruise $L = W$		0.000	0.000	1.6×10^{-8}	$[-4.7 \times 10^{-9}, -4.7 \times 10^{-9}, -4.7 \times 10^{-9}, -4.7 \times 10^{-9}, -4.7 \times 10^{-9}]$	—	-1.4×10^{-10}
	climb $L = W$		0.000	0.000	—	—	—	-8.3×10^{-11}

		Unit	Lower	Upper	Single-point	Multipoint	Mission-based	Single-point + climb
minimize	mission fuel burn	kg			11,173.83	11,168.74	11,141.58	11,164.54
w.r.t.	aspect ratio			10.401	**10.401**	**10.401**	**10.401**	**10.401**
	taper ratio				0.155	0.162	0.158	0.161
	sweep	deg			22.447	22.747	22.674	23.070
	twist	deg			[0.000, 5.138, -3.695, 0.393]	[0.000, 5.130, -3.615, 0.490]	[0.000, 4.616, -3.828, 0.185]	[0.000, 5.078, -3.327, 0.678]
	t/c ratio		0.030		[**0.030**, 0.096, 0.088, 0.114]	[**0.030**, 0.094, 0.088, 0.115]	[**0.030**, 0.093, 0.093, 0.119]	[0.030, 0.100, 0.093, 0.123]
	spar thickness	mm	3.000		[7.594, **3.000**, 6.046, 5.668]	[5.704, 3.734, 6.020, 5.612]	[7.509, **3.000**, 5.594, 5.102]	[6.219, **3.000**, 5.679, 5.215]
	skin thickness	mm	3.000		[6.298, 13.047, 18.391, 18.897]	[5.727, 13.382, 18.183, 18.891]	[6.081, 12.778, 16.670, 17.185]	[5.248, 12.492, 16.812, 17.560]
	maneuver AoA	deg			10.848	10.382	—	10.132
	cruise AoA	deg			7.40	[7.37, 7.19, 7.55, 7.04, 7.71]	—	7.04
	climb AoA	deg			—	—	—	10.514
subject to	2.5g failure			0.000	1.4×10^{-6}	2.1×10^{-8}	4.6×10^{-8}	1.4×10^{-7}
	maneuver $L = W$		0.000	0.000	-1.2×10^{-9}	-3.1×10^{-10}	—	6.9×10^{-9}
	cruise $L = W$		0.000	0.000	1.8×10^{-8}	$[1.5 \times 10^{-10}, 1.5 \times 10^{-10}, 1.5 \times 10^{-10}, 1.5 \times 10^{-10}, 1.5 \times 10^{-10}]$	—	6.7×10^{-9}
	climb $L = W$		0.000	0.000	—	—	—	6.2×10^{-9}

		Unit	Lower	Upper	Single-point	Multipoint	Mission-based	Single-point + climb
minimize	mission fuel burn	kg			20,345.36	20,338.33	20,297.51	20,335.74
w.r.t.	aspect ratio			10.401	**10.401**	**10.401**	**10.401**	**10.401**
	taper ratio				0.140	0.146	0.137	0.145
	sweep	deg			21.496	21.853	21.271	21.785
	twist	deg			[0.000, 4.786, -3.656, 0.172]	[0.000, 4.797, -3.647, 0.262]	[0.000, 4.033, -3.943, -0.257]	[0.000, 4.821, -3.388, 0.391]
	t/c ratio		0.030		[0.031, 0.096, 0.086, 0.112]	[0.032, 0.092, 0.089, 0.112]	[**0.030**, 0.092, 0.088, 0.113]	[0.031, 0.099, 0.088, 0.117]
	spar thickness	mm	3.000		[6.391, 3.306, 6.034, 5.696]	[6.394, **3.000**, 6.172, 5.660]	[8.009, **3.000**, 5.828, 5.278]	[6.057, **3.000**, 5.989, 5.415]
	skin thickness	mm	3.000		[7.025, 12.508, 18.246, 18.500]	[6.311, 13.303, 17.558, 18.604]	[7.742, 12.004, 17.329, 17.144]	[6.277, 12.110, 17.510, 17.664]
	maneuver AoA	deg			10.851	10.410	—	10.193
	cruise AoA	deg			7.10	[7.09, 6.92, 7.26, 6.78, 7.42]	—	6.78
	climb AoA	deg			—	—	—	10.614
subject to	2.5g failure			0.000	3.3×10^{-7}	1.3×10^{-8}	2.0×10^{-6}	8.1×10^{-9}
	maneuver $L = W$		0.000	0.000	1.0×10^{-9}	-5.6×10^{-10}	—	-2.3×10^{-10}
	cruise $L = W$		0.000	0.000	-5.3×10^{-9}	$[-3.0 \times 10^{-10}, -3.0 \times 10^{-10}, -3.0 \times 10^{-10}, -3.0 \times 10^{-10}, -3.0 \times 10^{-10}]$	—	-1.8×10^{-10}
	climb $L = W$		0.000	0.000	—	—	—	-1.4×10^{-10}

Table 8: Optimization results for the 300 nmi (top), 1,500 nmi (middle), and 2,900 nmi (bottom) missions

Acknowledgments

The first author is supported by the Department of Defense (DoD) through the National Defense Science and Engineering Graduate (NDSEG) Fellowship Program and in part by the Michigan Institute for Computational Discovery and Engineering (MICDE) Graduate Fellowship program. The first author would also like to thank Alasdair Christison Gray and Adam Wasserman for their insightful comments and suggestions.

References

[1] Haftka, R. T., "Optimization of Flexible Wing Structures Subject to Strength and Induced Drag Constraints," *AIAA Journal*, Vol. 15, No. 8, 1977, pp. 1101–1106. https://doi.org/10.2514/3.7400.

[2] Kenway, G. K. W., Kennedy, G. J., and Martins, J. R. R. A., "Aerostructural Optimization of the Common Research Model Configuration," *15th AIAA/ISSMO Multidisciplinary Analysis and Optimization Conference*, Atlanta, GA, 2014. https://doi.org/10.2514/6.2014-3274, aIAA 2014-3274.

[3] Martins, J. R. R. A., Alonso, J. J., and Reuther, J. J., "High-Fidelity Aerostructural Design Optimization of a Supersonic Business Jet," *Journal of Aircraft*, Vol. 41, No. 3, 2004, pp. 523–530. https://doi.org/10.2514/1.11478.

[4] Kenway, G. K. W., and Martins, J. R. R. A., "Multipoint High-Fidelity Aerostructural Optimization of a Transport Aircraft Configuration," *Journal of Aircraft*, Vol. 51, No. 1, 2014, pp. 144–160. https://doi.org/10.2514/1.C032150.

[5] Yanto, J., and Liem, R. P., "Aircraft fuel burn performance study: A data-enhanced modeling approach," *Transportation Research Part D: Transport and Environment*, Vol. 65, 2018, p. 574–595. https://doi.org/10.1016/j.trd.2018.09.014.

[6] Kroo, I., and Shevell, R., "Aircraft design: Synthesis and analysis," *Desktop Aeronautics Inc., Textbook Version 0.99*, 2001.

[7] Lee, H., and Chatterji, G. B., "Closed-Form Takeoff Weight Estimation Model for Air Transportation Simulation," *10th AIAA Aviation Technology, Integration, and Operations (ATIO) Conference*, Fort Worth, TX, 2010. https://doi.org/10.2514/6.2010-9156.

[8] Bons, N. P., Mader, C. A., Martins, J. R. R. A., Cuco, A. P. C., and Odaguil, F. I. K., "High-Fidelity Aerodynamic Shape Optimization of a Full Configuration Regional Jet," *2018 AIAA/ASCE/AHS/ASC Structures, Structural Dynamics, and Materials Conference*, Kissimmee, FL, 2018. https://doi.org/10.2514/6.2018-0106.

[9] Liem, R. P., Mader, C. A., Lee, E., and Martins, J. R. R. A., "Aerostructural design optimization of a 100-passenger regional jet with surrogate-based mission analysis," *2013 Aviation Technology, Integration, and Operations Conference*, 2013. https://doi.org/10.2514/6.2013-4372.

[10] Bons, N. P., "High-fidelity Wing Design Exploration with Gradient-based Optimization," Ph.D. thesis, University of Michigan, Ann Arbor, MI, May 2020.

[11] Chau, T., and Zingg, D., "Fuel burn evaluation of a transonic strut-braced-wing regional aircraft through multipoint aerodynamic optimisation," *The Aeronautical Journal*, 2022, pp. 1–25. https://doi.org/10.1017/aer.2022.64.

[12] Clarke, M. A., Erhard, R. M., Smart, J. T., and Alonso, J., "Aerodynamic Optimization of Wing-Mounted Propeller Configurations for Distributed Electric Propulsion Architectures," *AIAA Aviation 2021 Forum*, American Institute of Aeronautics and Astronautics, 2021. https://doi.org/10.2514/6.2021-2471, URL http://arc.aiaa.org/doi/10.2514/6.2021-2471.

[13] Jasa, J. P., Hwang, J. T., and Martins, J. R. R. A., "Open-source coupled aerostructural optimization using Python," *Structural and Multidisciplinary Optimization*, Vol. 57, No. 4, 2018, pp. 1815–1827. https://doi.org/10.1007/s00158-018-1912-8.

[14] Brelje, B. J., and Martins, J. R. R. A., "Development of a Conceptual Design Model for Aircraft Electric Propulsion with Efficient Gradients," *Proceedings of the AIAA/IEEE Electric Aircraft Technologies Symposium*, Cincinnati, OH, 2018. https://doi.org/10.2514/6.2018-4979.

[15] McCullers, L. A., "Aircraft configuration optimization including optimized flight profiles," *NASA. Langley Research Center Recent Experiences in Multidisciplinary Analysis and Optimization, Part 1*, 1984, pp. 395–412. N87-11743.

[16] Welstead, J. R., Caldwell, D., Condotta, R., and Monroe, N., "An Overview of the Layered and Extensible Aircraft Performance System (LEAPS) Development," *2018 AIAA Aerospace Sciences Meeting*, 2018.

[17] Botero, E. M., Wendorff, A., MacDonald, T., Variyar, A., Vegh, J. M., Lukaczyk, T. W., Alonso, J. J., Orra, T. H., and Ilario da Silva, C., "SUAVE: An open-source environment for conceptual vehicle design and optimization," *54th AIAA aerospace sciences meeting*, 2016.

[18] Trawick, D., Perullo, C., Armstrong, M., Snyder, D., Tai, J. C. M., and Mavris, D. N., "Development and application of GT-HEAT for the electrically variable engine (TM) design," *55th AIAA Aerospace Sciences Meeting*, 2017. https://doi.org/10.2514/6.2017-1922.

[19] Botero, E. M., and Alonso, J. J., "Conceptual design and optimization of small transitioning uavs using SUAVE," *18th AIAA/ISSMO Multidisciplinary Analysis and Optimization Conference*, 2017, p. 4149.

[20] Brelje, B. J., Jasa, J. P., Martins, J. R. R. A., and Gray, J. S., "Development of a Conceptual-Level Thermal Management System Design Capability in OpenConcept," *NATO Research Symposium on Hybrid/Electric Aero-Propulsion Systems for Military Applications (AVT-RSY-323)*, Trondheim, NO, 2019. https://doi.org/10.14339/STO-MP-AVT-323.

[21] Adler, E. J., Brelje, B. J., and Martins, J. R. R. A., "Thermal Management System Optimization for a Parallel Hybrid Aircraft Considering Mission Fuel Burn," *Aerospace*, Vol. 9, No. 5, 2022. https://doi.org/10.3390/aerospace9050243.

[22] Gladin, J. C., Trawick, D., Perullo, C., Tai, J. C., and Mavris, D. N., "Modeling and design of a partially electric distributed aircraft propulsion system with GT-HEAT," *55th AIAA Aerospace Sciences Meeting*, 2017.

[23] Liem, R. P., Kenway, G. K. W., and Martins, J. R. R. A., "Multimission Aircraft Fuel Burn Minimization via Multipoint Aerostructural Optimization," *AIAA Journal*, Vol. 53, No. 1, 2015, pp. 104–122. https://doi.org/10.2514/1.J052940.

[24] Hwang, J. T., Jasa, J. P., and Martins, J. R. R. A., "High-fidelity design-allocation optimization of a commercial aircraft maximizing airline profit," *Journal of Aircraft*, Vol. 56, No. 3, 2019, pp. 1164–1178.

[25] Variyar, A., Economon, T. D., and Alonso, J. J., "Multifidelity conceptual design and optimization of strut-braced wing aircraft using physics based methods," *54th AIAA Aerospace Sciences Meeting*, 2016.

[26] Jasa, J. P., Hwang, J. T., and Martins, J. R. R. A., "Design and trajectory optimization of a morphing wing aircraft," *2018 AIAA/ASCE/AHS/ASC Structures, Structural Dynamics, and Materials Conference*, 2018, p. 1382.

[27] Gray, J. S., Hwang, J. T., Martins, J. R. R. A., Moore, K. T., and Naylor, B. A., "OpenMDAO: An open-source framework for multidisciplinary design, analysis, and optimization," *Structural and Multidisciplinary Optimization*, Vol. 59, No. 4, 2019, pp. 1075–1104. https://doi.org/10.1007/s00158-019-02211-z.

[28] Hwang, J. T., and Martins, J. R. R. A., "A computational architecture for coupling heterogeneous numerical models and computing coupled derivatives," *ACM Transactions on Mathematical Software*, Vol. 44, No. 4, 2018, p. Article 37. https://doi.org/10.1145/3182393.

[29] Hendricks, E. S., and Gray, J. S., "pyCycle: A Tool for Efficient Optimization of Gas Turbine Engine Cycles," *Aerospace*, Vol. 6, No. 87, 2019. https://doi.org/10.3390/aerospace6080087.

[30] Lambe, A. B., and Martins, J. R. R. A., "Extensions to the Design Structure Matrix for the Description of Multidisciplinary Design, Analysis, and Optimization Processes," *Structural and Multidisciplinary Optimization*, Vol. 46, No. 2, 2012, pp. 273–284. https://doi.org/10.1007/s00158-012-0763-y.

[31] Nita, M., and Scholz, D., "Estimating the Oswald Factor from Basic Aircraft Geometrical Parameters," *Deutscher Luft- und Raumfahrtkongress*, Berlin, Germany, 2012.

[32] Raymer, D. P., *Aircraft Design: A Conceptual Approach*, American Institute of Aeronautics and Astronautics, 1992.

[33] Chauhan, S. S., and Martins, J. R. R. A., "Low-Fidelity Aerostructural Optimization of Aircraft Wings with a Simplified Wingbox Model Using OpenAeroStruct," *Proceedings of the 6th International Conference on Engineering Optimization, EngOpt 2018*, Springer, Lisbon, Portugal, 2018, pp. 418–431. https://doi.org/10.1007/978-3-319-97773-7_38.

[34] Brooks, T. R., Kenway, G. K. W., and Martins, J. R. R. A., "Undeflected Common Research Model (uCRM): An Aerostructural Model for the Study of High Aspect Ratio Transport Aircraft Wings," *18th AIAA/ISSMO Multidisciplinary Analysis and Optimization Conference*, Denver, CO, 2017. https://doi.org/10.2514/6.2017-4456.

[35] Virtanen, P., Gommers, R., Oliphant, T. E., Haberland, M., Reddy, T., Cournapeau, D., Burovski, E., Peterson, P., Weckesser, W., Bright, J., van der Walt, S. J., Brett, M., Wilson, J., Millman, K. J., Mayorov, N., Nelson, A. R. J., Jones, E., Kern, R., Larson, E., Carey, C. J., Polat, b., Feng, Y., Moore, E. W., VanderPlas, J., Laxalde, D., Perktold, J., Cimrman, R., Henriksen, I., Quintero, E. A., Harris, C. R., Archibald, A. M., Ribeiro, A. H., Pedregosa, F., van Mulbregt, P., and SciPy 1.0 Contributors, "SciPy 1.0: Fundamental Algorithms for Scientific Computing in Python," *Nature Methods*, Vol. 17, 2020, pp. 261–272. https://doi.org/10.1038/s41592-019-0686-2.

[36] Liem, R. P., Mader, C. A., and Martins, J. R. R. A., "Surrogate Models and Mixtures of Experts in Aerodynamic Performance Prediction for Aircraft Mission Analysis," *Aerospace Science and Technology*, Vol. 43, 2015, pp. 126–151. https://doi.org/10.1016/j.ast.2015.02.019.

[37] Kao, J. Y., Hwang, J. T., Martins, J. R. R. A., Gray, J. S., and Moore, K. T., "A Modular Adjoint Approach to Aircraft Mission Analysis and Optimization," *Proceedings of the AIAA Science and Technology Forum and Exposition (SciTech)*, Kissimmee, FL, 2015. AIAA 2015-0136.

[38] Kreisselmeier, G., and Steinhauser, R., "Systematic Control Design by Optimizing a Vector Performance Index," *International Federation of Active Controls Symposium on Computer-Aided Design of Control Systems, Zurich, Switzerland*, 1979. https://doi.org/10.1016/S1474-6670(17)65584-8.

[39] Lambe, A. B., Martins, J. R. R. A., and Kennedy, G. J., "An Evaluation of Constraint Aggregation Strategies for Wing Box Mass Minimization," *Structural and Multidisciplinary Optimization*, Vol. 55, No. 1, 2017, pp. 257–277. https://doi.org/10.1007/s00158-016-1495-1.

[40] Kenway, G. K. W., and Martins, J. R. R. A., "Multipoint Aerodynamic Shape Optimization Investigations of the Common Research Model Wing," *AIAA Journal*, Vol. 54, No. 1, 2016, pp. 113–128. https://doi.org/10.2514/1.J054154.

[41] Gill, P. E., Murray, W., and Saunders, M. A., "SNOPT: An SQP Algorithm for Large-Scale Constrained Optimization," *SIAM Review*, Vol. 47, No. 1, 2005, pp. 99–131. https://doi.org/10.1137/S0036144504446096.

[42] Roskam, J., *Airplane Design*, 2nd ed., Vol. 1-8, DARCorporation, Ottawa, KS, 1998.

[43] Chiba, K., Obayashi, S., and Nakahashi, K., "High-Fidelity Multidisciplinary Design Optimization of Aerostructural Wing Shape for Regional Jet," *Proceedings of the 23rd AIAA Applied Aerodynamics Conference*, Toronto, ON, Canada, 2005.

[44] Hale, F. J., "Best-range flight conditions for cruise-climb flight of a jet aircraft," *NASA. Langley Res. Center Advan. in Eng. Sci., Vol. 4*, 1976.